Study on the thermal and mechanical properties of novel neutron shielding composite laminates at elevated temperature

Xue-Long Fu[a,b,c], Yu-Bing Hu[a,c], Hua-Guan Li[a,c], Jie Tao[a,c,*]

[a.]College of Material Science & Technology, Nanjing University of Aeronautics & Astronautics, Nanjing 211106, China;

[b.]Department of Mechanical & Electronic Engineering, Jiangsu Polytechnic of Finance & Economics, Huai'an, Jiangsu 223003, China;

[c.]Jiangsu Collaborative Innovation Center for Advanced Inorganic Function Composites, Nanjing 211106, China;

Abstract: Neutron shielding fibre metal laminates (NSFMLs) containing 10-50wt% of boron carbide (B_4C) powder were fabricated using hot molding process, and the effects of experimental temperature on the thermal and mechanical properties of composite laminates were investigated in this work. Thermal stability of composite laminates was conducted with thermo-gravimetric analysis (TGA) and differential scanning calorimetry (DSC), and their mechanical properties were also measured. The testing results indicated that good interfacial adhesion between different layers, uniform distribution of B_4C particles and carbon fibres tightly surrounded by polyimide (PI) resin were crucial to the mechanical properties of composite laminates. TGA-DSC results illustrated the scarcely mass loss of composite laminates below 300 ℃, yet began to decompose when it exceeded over 390 ℃. Moreover, tensile strength of the NSFMLs degraded with the increasing of experimental temperature and the volume fraction of B_4C powder. Double bear shear (DBS) testing results showed that the NSFMLs with 30wt% of B_4C powder had the maximum interlaminar shear value, while the primary delamination zone occurred at the interface between two layered carbon fibre reinforced prepregs (CFRPs). The composite laminates still maintained the good interlaminar shear strength even at 300 ℃.

Keywords: Neutron shielding fibre metal laminates (NSFMLs); Thermal properties; Interlaminar shear (ILS) strength; Hot molding process

1. Introduction

With the increasing requirements in energy to satisfy the basic survival and development needs of human beings, energy structure of coal-fired power generation brings great challenges to the ecological environment, making people's attention paid on other clean energy resources, such as nuclear energy. The main reason lies in that nuclear energy is the cleanest and most cost-effective power resources presently, and more than 15% of the world's electricity comes from nuclear power plants (NPPs) [1-3]. Although nuclear fuel could not yield carbon dioxide or other harmful greenhouse gas emissions, it creates its own waste in the form of highly radioactive spent nuclear fuel enriched in the fissile ^{235}U [4]. All types of radioactive wastes need to be carefully managed so as to keep the public safe, protect the environment and ensure the security from accidental or deliberate intrusion [5-7]. Normally, there are two primary byproducts, including the spent nuclear fuel (SNF) from nuclear reactors and high-level waste from the reprocessing of spent nuclear fuel, and how to cope with such byproducts is the first problem facing the scientists around the world [8]. Usually, the measurements taken are concentrated on the management, conservation and direct reusage of SNF, to ensure the safety management of the NPPs [9].

* Corresponding author: College of Material Science & Technology, Nanjing University of Aeronautics and Astronautics, Nanjing, China. Tel.: +086 13347800587; Fax: +86 025 52112911. E-mail address: taojie@nuaa.edu.cn (J. Tao)

Considering the high radioactivity of SNF, the disposal of radioactive nuclear waste must be carefully arranged. It is correlated with the storage of SNF regardless of what measures are taken in the nuclear engineering. For the storage of the SNF generated from the NPPs, neutron shielding materials should have good thermal and mechanical properties, in addition to good neutron shielding performance and radiation resistance, to satisfy the requirements for structural function. Presently, there are three main heatproof neutron shielding resins available, e.g. 90 ℃ in polyethylene (PE), 150 ℃ in KRAFTON [10] and 200 ℃ in EPONITE [11]. The most widely used nuclear protective material is polyethylene-based composite with the addition of ^{10}B-containing substances (particles or fibres), to make full use of hydrogen atoms contained in the polyethylene as an effective neutron moderator and ^{10}B atoms in boron carbide as a good thermal neutron absorber [12,13]. However, PE plastic plates, as a protective material, have its shortcomings of applied temperature below 100 ℃, limiting the scope of its application. For the needs of applying at elevated temperature such as nuclear reactor, especially in light of radiation accidents, polyethylene plastic plate may lose its protective function. Therefore, it is imperative to find out the substitutes having the optimum thermal stability and wide usage temperature range. Polyimide (PI) resin reported in the literature [14] has good dimensional stability and good adhesion at elevated temperature, and it also has high creep resistance and radiation resistance (5 $\times 10^9$ rad), which can be a good candidate for neutron shielding materials. On the other hand, the corresponding wettability between PI resin and carbon fibre is very good, ensuring the better mechanical performance of carbon fibre reinforced polyimide composite.

In this study, neutron shielding fibre metal laminates (NSFMLs) with a 3/2 configuration, consisting of three AA6061 alloy plates coated with neutron shielding composite (NSC) and two carbon fibre reinforced polyimide (CFRP) layers, were fabricated using hot molding process. Microstructures of the NSFMLs with various contents of B_4C particles were performed to evaluate the interfacial bonding characteristics of the constituents in the NSFMLs. Thermogravimetric analysis (TGA) and differential scanning calorimetry (DSC) of the specimens were measured, and thermal conductivities were also studied to acquire the heat transfer performance; moreover, tensile and interlaminar shear (ILS) properties of the NSFMLs at elevated temperature were conducted as a function of the experimental temperature.

2. Experimental procedure

2.1 Materials

AA6061 alloy plates (0.5 mm in thickness, Southwest Aluminum (Group) Co. Ltd., China), nuclear grade boron carbide (B_4C) particles (7.5 μm in average particle size, 99.5% purity, Jingangzuan Boron Carbide Co. Ltd., Mudanjiang, China), carbon fibre (TR50S 6K, Mitsubishi Rayon Co. Ltd., China) and PMR polyimide resin (KH-308, Institute of Chemistry, Chinese Academy of Science, Beijing, China) were used as raw materials. SEM micrograph and relative XRD pattern of B_4C particulates are presented in Fig.1. The PMR polyimide with the solution viscosity of 56.8 mPa.s contains about 50wt% of polymerized reaction mixtures. Carbon fibre reinforced prepregs (CFRPs) with 0.125 mm in thickness, which were composed of carbon fibre and PMR polyimide, were self-prepared by numerical control automatic placement machine in the laboratory [15].

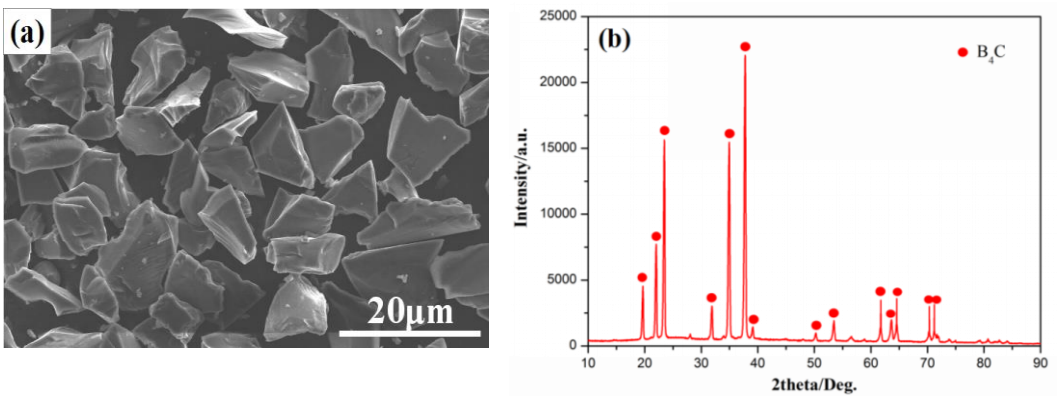

Fig. 1 (a) SEM image and (b) XRD pattern of boron carbide particulates

2.2 Preparing process

AA6061 alloy plates were firstly anodized by phosphoric acid according to the standard procedures [16], and then coated with neutron shielding composite with 0.2±0.02 mm in thickness which was composed of the mixture of PMR polyimide and nuclear-grade B_4C particles. The contents of B_4C particles contained in the neutron shielding composite layer were 10wt%, 20wt%, 30wt%, 40wt% and 50wt%, respectively. In order to improve the interfacial bonding between B_4C particles and PI resin, alkoxysilane (KH550) coupling agents were added into the solution. AA6061 plates coated with neutron shielding composite were then put into the drying oven at 60 ℃ for 12 hrs to get rid of the solvent in the PI resin. After completing the whole process mentioned above, the specimens were laminated with carbon fibre reinforced prepregs. Each prepreg layer was composed by two unidirectional (UD) carbon fiber prepreg oriented in 0 °layer, which was coincident with the rolling direction of AA6061 plates. The schematic illustration of preparing process of composite laminates is exhibited in Fig.2, and the detailed preparing process is available in the literature [17].

The neutron shielding fibre metal laminates (NSFMLs) with a 3/2 configuration, composed of stacking layer of AA6061 plates, neutron shielding composite (NSC) and carbon fibre reinforced polyimide (CFRP), were firstly stacked in the compression mold by hand lay-up, and then placed into the vulcanizing machine, and finally hot compressed under the pressure of 2-3 MPa when the mold temperature exceeded 280 ℃. The explicit curing process of all composite laminates was 80 ℃ for 1 hr, 120 ℃ for 1 hr , 160 ℃ for 1 hr, 200 ℃ for 1 hr, 280 ℃ for 1/2 hr, and 320 ℃ for 2 hrs. The NSFMLs with 10-50 wt% of B_4C particles, notated as ABP10, ABP20, ABP30, ABP40 and ABP50, were fabricated in accordance with the curing process, correspondingly. After the curing procedure, packing pressure should be maintained in order to alleviate the effect of residual strength, caused by discrepancy in the coefficient of thermal expansion (CTE) between different components, on the mechanical properties of the NSFMLs. The specimens with desired shapes and dimensions were cut for mechanical and other evaluations with high precision Struers Secotom-15 Cutter (cutting tool: diamond saw blade, 200 mm × 0.8 mm × 22 mm; feed rate: 0.15-0.25 mm/s; rotation speed: 3200 rpm).

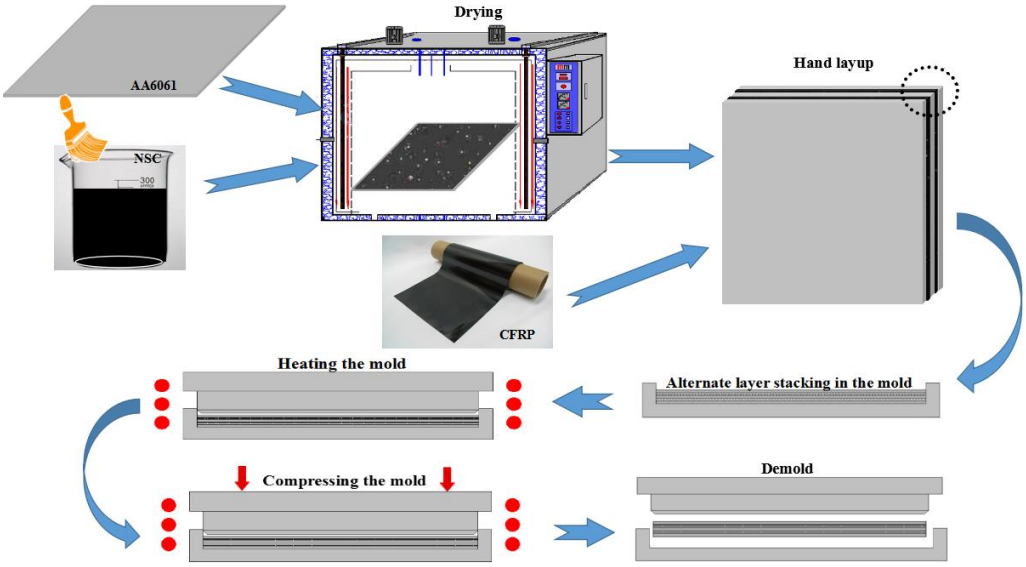

Fig.2 Schematic illustration of preparing process of the NSFMLs

2.3 Thermal behavior

2.3.1 Thermogravimetric analysis (TGA)

Thermal stability of the NSFMLs with different fractions of B_4C particles was investigated using a simultaneous thermal analysis (STA 409, NETZSCH) of both thermogravimetric analysis (TGA) and differential scanning calorimetry (DSC) at a flow rate of 100 ml/min under nitrogen and air atmosphere. Analysis was carried out in the alumina crucible, with the temperature ranging from 25 ℃ to 750 ℃ at a heating rate of 10 ℃ min^{-1}. All tests were repeated once.

2.3.2 Thermal conductivity (TC)

Thermal conductivities of the NSFMLs were conducted using DRL-Ⅱ thermal conductivity tester (Xiangtang Xiangke Instrument Co., Ltd.) in accordance with ASTM D5470-12 [18]. The specimens with 30 ± 0.1 mm in diameter were tested, and the testing instrument has the capacity of thermal conductivity ranging from 0.015 to 45 W/m k with the precision of 3% under vacuum atmosphere. The schematic diagram of testing instrument is illustrated in Fig.3.

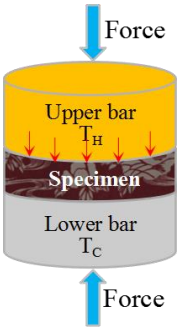

Fig.3 Schematic diagram of thermal conductivity testing instrument

Thermal conductivities (λ) of composite laminates as an indicator can be evaluated using the following equation:

$$\lambda = \frac{A}{Q} \times (T_H - T_C) \tag{1}$$

Where A is the area of the reference calorimeter /m^2, Q is the average heat flow through specimen, T_H and T_C are the temperature of hot and cold meter bar surface in contact with the specimen respectively /K.

2.4 Mechanical testing

The tests of tensile and interlaminar shear (ILS) properties were conducted on the CMT-5015 Universal Testing Machine (UTM) in displacement control. The testing process of the specimens with the dimensions of 200 mm × 12.5 mm × (2.7±0.15) mm was monitored by extensometer in order to precisely measure the change of stress-strain curve, in accordance with ASTM D3039 at a displacement rate of 2 mm/min, and the experimental specimens were put into the environmental chamber for 5 mins. The experimental temperature was maintained at 25 ℃, 100 ℃, 200 ℃ and 300 ℃, respectively. Interlaminar shear (ILS) strength of composite laminates was performed with double beam shear (DBS) method reported in the literature [19], with a span-to-thickness ratio (L/h) of 5 at a crosshead displacement rate of 1 mm/min. The experimental setup of double beam shear testing is presented in Fig.4. The theoretical load analysis of bending stress and interlaminar shear characteristic for the testing specimen is exhibited in Fig.5, and 's' represents the distance between the outer applying point and the inner point where the bending stress is zero. The interlaminar shear strength (τ) was calculated using the following equation:

$$\tau = \frac{33P_{crit}}{64bt} \tag{2}$$

Where P_{crit} is the critical strength obtained from the UTM machine, b and t are the width and thickness of the specimens, respectively.

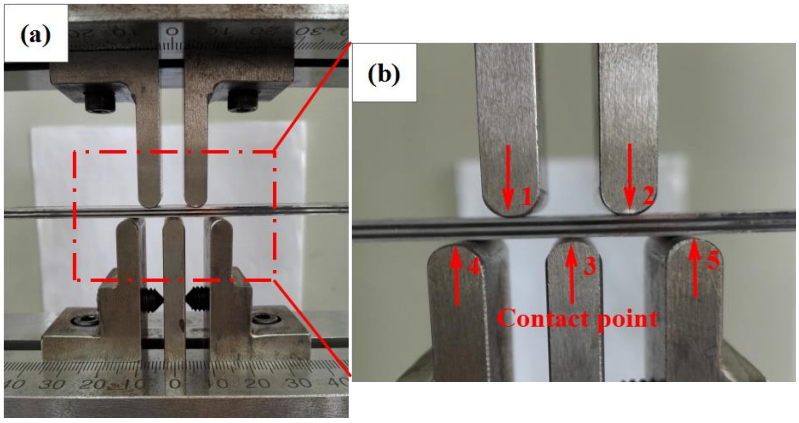

Fig.4 Experimental setup of double beam shear (DBS) testing: (a) low and (b) high magnification

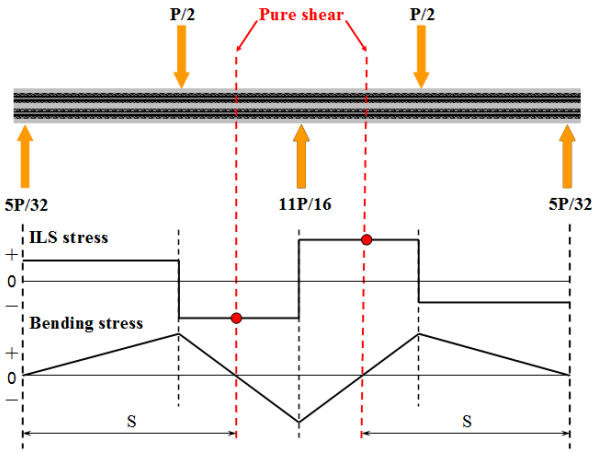

Fig.5 Load analysis of composite laminates under double beam shear testing method

2.5 Morphology characterization

Microstructures of the NSFMLs with various contents of B_4C particles were characterized using optical microscope (OM, Leica DM IL LED, Germany) and field emission scanning electron microscopy (FE-SEM, Quanta 250 FEG, FEI, America) equipped with energy-dispersive spectroscopy (EDS, Oxford INCA energy). The fractured portions of the specimens were cut and gold-coated uniformly on the surface for examination, and the accelerating voltage used in this work was 10 kV. Crystalline phases of B_4C particles were examined using X-ray diffractometry (XRD, Ultimate IV, Rigaku, Japan) with the scanning angle ranging from 10 degree to 90 degree.

3. Results and discussion

3.1 Microstructures

Figure 6 illustrates the SEM micrograph of the surface of AA6061 alloy plate after anodizing process. A lot of shallow holes are presented on the surface of AA6061 plates when compared with the as-received materials, which is beneficial for the interfacial adhesion between AA6061 plate and neutron shielding composite (NSC). In other words, the rough surface of AA6061 alloy plate is conducive to improve the adhesive bonding, interlaminar shear strength of the NSFMLs.

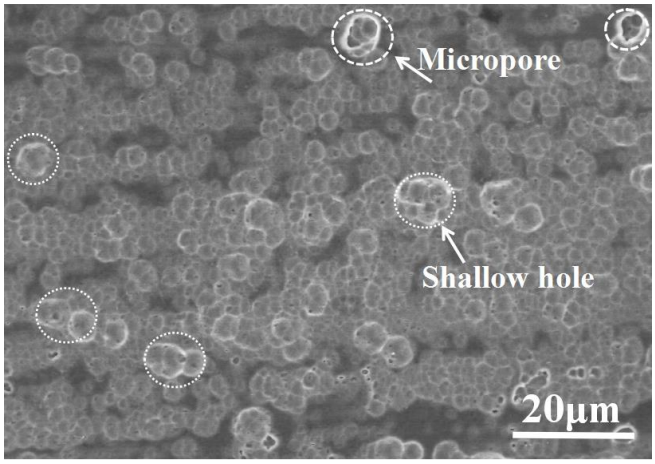

Fig.6 SEM micrograph of AA6061 plate after anodizing process

Microstructures of polished NSFMLs with various contents of B_4C particles are shown in Fig.7. It is indicated that, B_4C particles are uniformly dispersed in the PI resin after curing process, and no critical aggregation of B_4C particles is observed for all five concentrations. It is closely bonded along the interface between AA6061 alloy plate and PI resin as presented in Fig.7(a), and no significant gap or porosity appears at the interface. The black particles marked in Fig.7(a)-(e) are B_4C particles, and the light regions are AA6061 alloy plate and the black regions are PI resin. Moreover, B_4C particles are tightly surrounded by PI resin, increasing the resistance of neutron shielding particulates pulling out from PI resin and reducing the porosity of composite laminates, which is essential for the mechanical and neutron shielding performance of composite laminates. Fig.7(f) exhibits the uniform distribution of carbon fibres in the composite laminates, and carbon fibres are closely enwrapped by PI resin, resulting in the good mechanical properties of the NSFMLs.

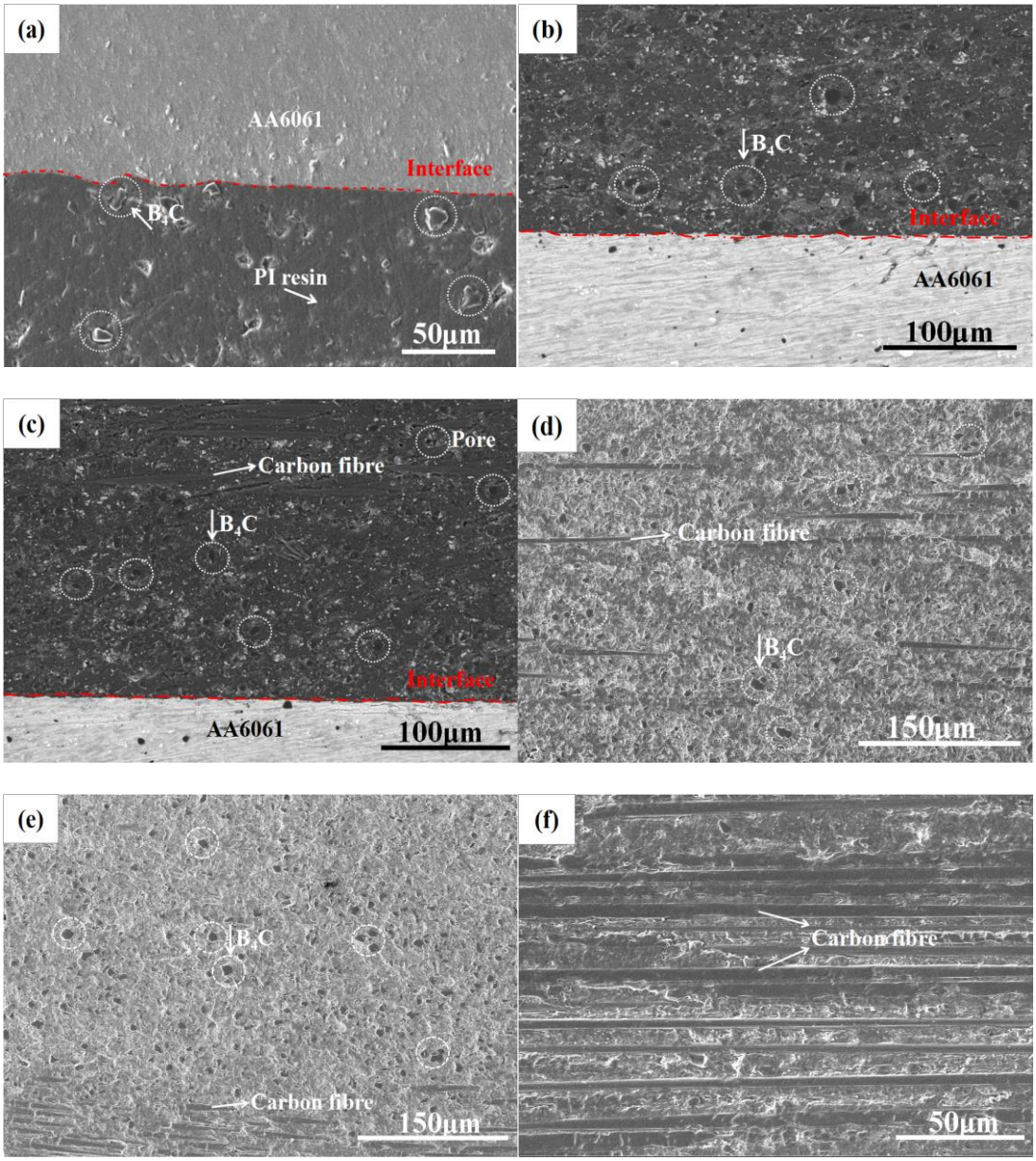

Fig.7 SEM images of polished composite laminates with different fractions of B_4C particles: (a) ABP10; (b) ABP20; (c) ABP30; (d) ABP40; (e) ABP50 and (f) distribution of carbon fibres

Fig. 8 exhibits the SEM micrograph of stripping surface of composite laminates with 30 wt% of B_4C particles. As shown in the figure, B_4C particles acting as neutron absorber are tightly surrounded by polyimide resin, which is a prerequisite for the good mechanical properties and neutron shielding performance of composite laminates, and the composite with high relative density can effectively block the penetration of neutrons. On the other hand, alkoxysilane coupling agent is beneficial for the interfacial adhesion between B_4C particles and polyimide resin, decreasing the porosity of laminated composite.

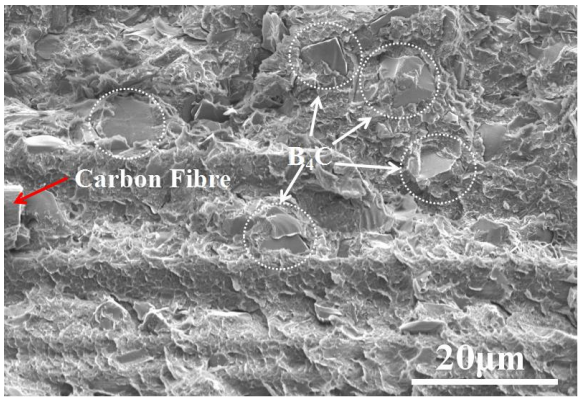

Fig.8 SEM micrograph of stripping surface of composite laminates with 30 wt% of B_4C particles

3.2 Thermal properties

3.2.1 Thermal stability analysis

Figure 9 shows the TGA-DSC curves of composite laminates containing different fractions of B_4C powder, with the temperature ranging from 25 ℃ to 650 ℃ at a heating rate of 10 ℃/min. As presented in Fig.9(a), all specimens maintain good thermal stability and scarcely lose mass when the experimental temperature is lower than 300 ℃, and the mass remaining of ABP10-ABP50 at 300 ℃ are 99.27%, 99.48%, 99.51%, 99.56% and 99.62%, of the initial weight, respectively. It is anticipated that, mass loss of the specimens is attributed to the removal of moisture contained in the NSFMLs. When the ambient temperature exceeds over 450 ℃, thermogravimetric curves of all specimens almost appear a obvious weight loss. When the calcination temperature approached to 650 ℃, weight reductions of the specimens with B_4C contents of 10, 20, 30, 40 and 50 wt.% are about 14.13%, 12.25%, 7.79%, 6.61% and 5.57%, respectively. After heat treated at 650 ℃, polyimide resin has obviously pyrolyzed and volatilized. But for the carbon fibres, as illustrated in the Fig.9(a), have no marked failure behavior; on the other hand, the interface of composite laminates has been severely broken owing to the pyrolysis of PI resin. The mass of the specimens calcined at 300 ℃ and 650 ℃ is shown in Table 1.

Accordingly, Fig.9(b) illustrates the DSC thermogram of composite laminates with the increasing of experimental temperature. Two peaks are presented in the heat flows of the NSFMLs in air, including one endothermic peak at 390 ℃ (notation: Peak 1) and another exothermic peak around at 615 ℃ (notation: Peak 2). By comparing the heat flows of composite laminates with various contents of B_4C particles in the neutron shielding layer, it can be concluded that the formation of endothermic peak 1 of the NSFMLs is caused via the initial decomposition temperature of composite laminates, and the initial transition temperature of composite laminates in nitrogen is around 390 ℃. The weight change caused by the oxidation of AA6061 alloy under air atmosphere is negligible when the temperature is lower than 400 ℃ owing to the protection of existed alumina on the surface of AA6061 plates. While peak 2 in Fig.9(b) is attributed to the oxidation of B_4C particles when combining the thermal stability of neat B_4C powder calcined with the increasing of temperature, which is further illustrated in Fig.10. The addition of B_4C particles decreases the chain mobility of PI resin, indicating a ~30 ℃ increase in the glass transition temperature (T_g) in comparison to neat PI resin.

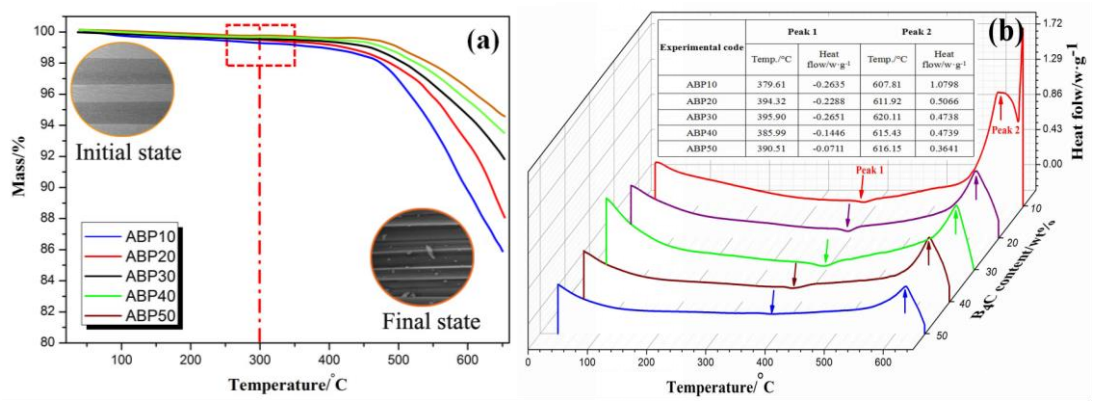

Experimental code	Peak 1		Peak 2	
	Temp./°C	Heat flow/w·g⁻¹	Temp./°C	Heat flow/w·g⁻¹
ABP10	379.61	-0.2635	607.81	1.0798
ABP20	394.32	-0.2288	611.92	0.5066
ABP30	395.90	-0.2651	620.11	0.4738
ABP40	385.99	-0.1446	615.43	0.4739
ABP50	390.51	-0.0711	616.15	0.3641

Fig.9 (a) Thermogravimetric analysis (TGA) and (b) differential scanning calorimetry (DSC) curves of composite laminates with various contents of boron carbide

Table 1 Mass remains of composite laminates at 300 ℃ and 650 ℃

Atmosphere	Heating rate /℃ min^{-1}	B_4C content /wt%	Mass/%	
			300 ℃	650 ℃
Air	10	10	99.27	85.87
		20	99.48	87.75
		30	99.51	92.21
		40	99.56	93.39
		50	99.62	94.43

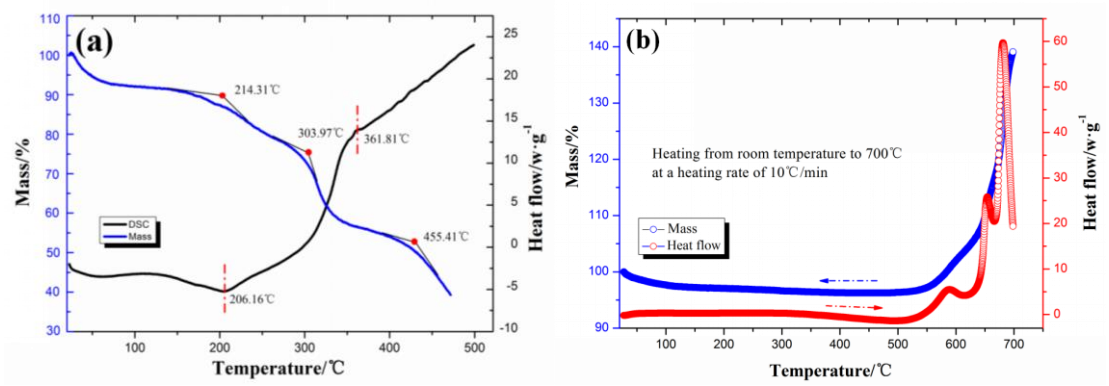

Fig.10 TGA-DSC curves of (a) neat PI resin and (b) B_4C particles as a function of temperature at a heating rate of 10 ℃/min

Fig.10(a) shows the TGA-DSC curve of neat KH-308 polymide resin pretreated at 120 ℃ for 12 hrs. The endothermic peak happened at 206.16 ℃ is attributed to the imidization, and the solvent is released during the imidization process. The conversion of polyamic acid to polyimide is almost completed after reaction at 303.97 ℃. For the comparison, data of a monolithic B_4C without other additives was also plotted, and TGA-DSC curve of neat B_4C particles as a function of experimental temperature at a heating rate of 10 ℃/min is exhibited in Fig. 10 (b). As shown in the figure, the mass of B_4C particles is almost unchanged until the temperature exceeds over 520 ℃. The oxidation behavior of boron carbide reported in open literature has happened on the surface of boron carbide, resulting in the formation of a thin transparent B_2O_3 film [20]. Normally, the thermal stability of composite laminates is affected by the changing of environment and temperature.

3.2.2 Thermal conductivity

Thermal conductivity (TC) dominates the heat transfer rate to guarantee the stability and safety of spent nuclear fuel, and heat exchange efficient is vital for the operation of nuclear system [21]. Figure 11 presents the thermal conductivity of composite laminates containing various fractions of B_4C particles. Normally, thermal conductivities of PI resin and B_4C powder are about 0.16 and 33.2 W/(m ·k) at room temperature. It can be clearly seen from the testing results that, thermal conductivities of the NSFMLs with different contents of B_4C particles ranging from 10 wt% to 50 wt% are 0.39, 0.45, 0.49, 0.53 and 0.55 W/(m ·k), respectively. Thermal conductivities of the NSFMLs are increased with the contents of B_4C particles. It is analyzed that, when the content of B_4C is low, the distances between B_4C particles distributed in the NSFMLs are so large that less thermal conductive channel and thermal conductive network is formed. But for the NSFMLs with higher fraction of B_4C particles, B_4C particles are inclined to approach to each other, resulting in the more chance to contact and interact between B_4C particulates, and more thermal conductive network comes into being, as a result, increasing the thermal conductivities of composite laminates. Generally, thermal conductivity of laminated composite is closely correlated with the structure, fraction and distribution of the components, and it is also depended on the porosity, interfacial characteristics of the NSFMLs in combination with the surrounding circumstances [22,23].

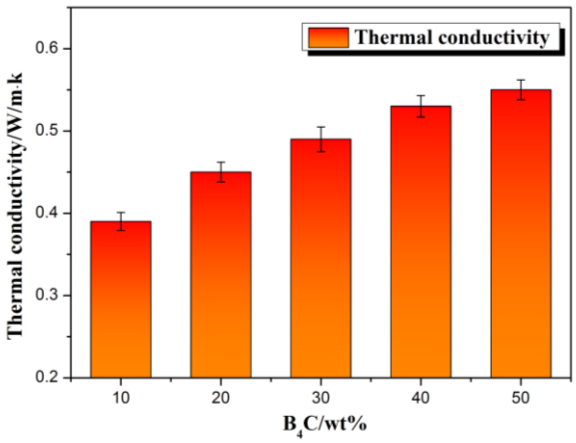

Fig.11 Thermal conductivity of the NSFMLs with various fractions of B_4C particles

3.3 Mechanical properties

3.3.1 Tensile properties

Figure 12 shows the tensile strength of AA6061 alloy plate and hybrid composite laminates with the increasing of experimental temperature. Tensile strength of the specimens is measured in accordance with ASTM D3039 at the displacement rate of 2 mm/min, and the experimental temperature ranges from room temperature (RT) to 300 ℃.

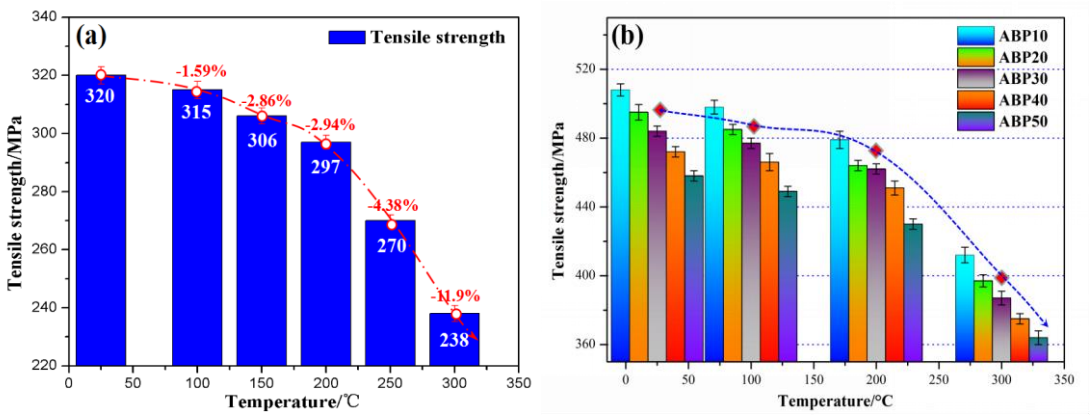

Fig.12 Effect of experimental temperature on the tensile strength of (a) AA6061 alloy plate and (b) composite laminates with different configurations

It can be clearly seen from Fig. 13(a) that tensile strength of AA6061 alloy plate decreases with the increasing of experimental temperature, and tensile strength tested at 300 ℃ is around 238 Mpa, which is about 74.4% of the initial value at room temperature. The decrease of tensile strength is associated with the grain growth in the AA6061 alloy due to the increase of temperature. Moreover, aluminum alloy applied over 150 ℃ for long-term service will usually cause the precipitation phase to grow up, and the yield strength of AA6061 alloy plate at elevated temperature is also affected by creep deformation [24]. On the other hand, laminated composite with 10wt% of B_4C particles has higher tensile strength than that with 50wt% of boron carbide powder, as shown in Fig.13 (b). That's because the NSFML with 10wt% of B_4C particles has better interfacial bonding strength than the latter, resulting in the higher ultimate yield strength of NSFMLs. Tensile strength of the specimens with five different concentrations exhibits an downward tendency as a function of experimental temperature, and the descending rate is relatively slow below 200 ℃. When the temperature exceeds over 200 ℃, tensile strength decreases obviously. Usually, tensile performance of the specimen is closely correlated with the interfacial bonding and volume fraction of the constituents, in accordance with the principle of metal volume fraction (MVF) [25]. After the addition of B_4C particles into the NSFMLs, glass transition temperature (T_g) of composite laminates increase correspondingly according to the analysis of TGA results mentioned above. However, when the experimental temperature exceeds the glass transition point of polyimide, PI resin will lose its supporting function, decreasing the overall mechanical performance of the NSFMLs. Consequently, the usage temperature of the NSFMLs should be limited below 390 ℃.

Figure 13 exhibits the SEM images of the NSFMLs with a 3/2 configuration after tensile tests. As shown in Fig.13(a), it is the macroscopic fractograph of the NSFMLs conducted at room temperature, and the fracture surface of neutron shielding composite layer is quite regular and flat. The delamination zone initiates on the interface between AA6061 plates and neutron shielding composite layer after the failure of composite laminates, and almost all specimens with five concentrations exhibit the analogous fracture characteristics. Normally, aluminum alloy plates have better ductility than neutron shielding composite and carbon fibres, that's the reason why the delamination comes into being. The composite laminates (in Fig.13(b) and (c)) tested at room temperature and 200 ℃ respectively, exhibit the substantial pullout of carbon fibres and matrix debonding, while the broken carbon fibres can also be observed at the fracture surface. Moreover, B_4C powder in the NSFMLs tightly surrounded by PI resin (Fig.13(e)), is essential to the good

thermal conductivities of composite laminates. Fig.13(f) illustrates the fractograph of AA6061 alloy plate, and the presence of dimples can be obviously observed, which is also the typical tensile characteristic of aluminum alloy materials.

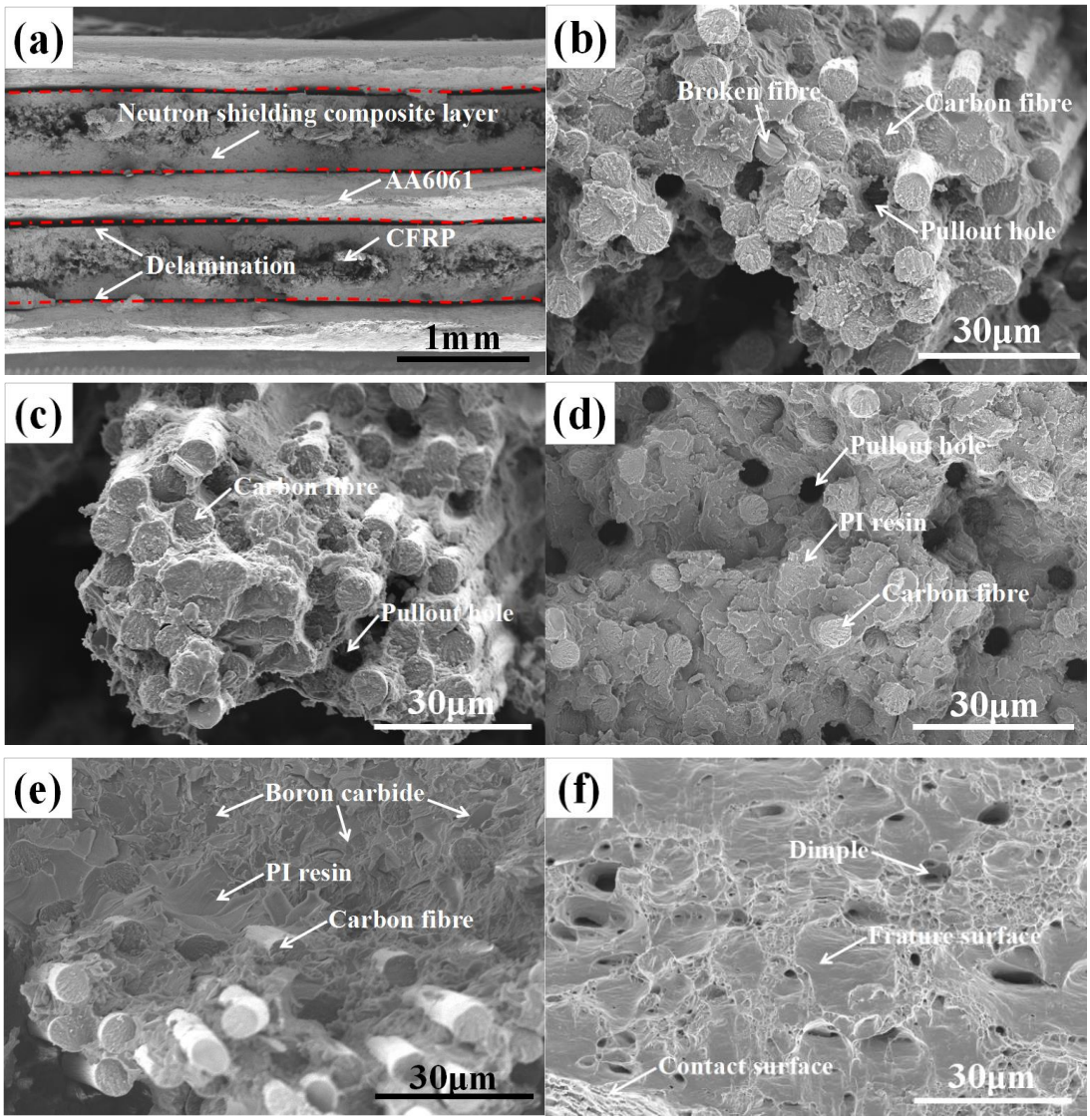

Fig.13 SEM images of the NSFMLs with a 3/2 configuration: (a) macroscopic fractograph; fracture morphology of the CFRP at (b) room temperature, (c) 200 ℃ and (d) 300 ℃; (e) fractograph of NSC layer; (f) fractograph of AA6061 alloy plate

3.3.2 Interlaminar shear (ILS) strength

The tests of interlaminar shear strength were conducted in accordance with the principle of double bear shear (DBS) testing, and the ILS strength testing results of the NSFMLs performed at different experimental temperature are presented in Fig.14. It can be clearly seen that, the NSFML with 30wt% of B_4C powder has the highest ILS strength when compared with other configurations. If further increasing the fraction of B_4C particles exceeding 30wt%, the ILS strength is inclined to decrease by virtue of the decreasing interfacial adhesion between neutron shielding composite layer and AA6061 plate. The main reason lies in that, the addition of B_4C particles acting as a pinning effect can improve the resistance of relative movement between AA6061 plate and neutron shielding composite (NSC) layer, resulting in the enhancement of interlaminar shear strength. When the content of B_4C particles in the NSC layer approaches 30wt%, the supporting

and pinning synergistic effect hits a high point with the maximum value of 95.55 MPa, as illustrated in Fig.15(a). On the other hand, if the fraction of B_4C particles exceeds over 30 wt%, the effective interfacial bonding between NSC layer and AA6061 plate tends to decrease, as a result, lessening the interlaminar shear strength of the NSFMLs with relatively higher fraction of B_4C particles. The ILS strength of composite laminates exhibits a downward tendency with the increase of experimental temperature, while the tendency is comparatively slow below 200 ℃, as indicated in Fig.14(a)-(c). The composite laminates conducted at 300 ℃ present the stable interlaminar shear strength, with the value accounting for about 70% of the initial value, which illustrates that the interfacial bonding between AA6061 plate and NSC layer is effective even at elevated temperature. Moreover, the interlaminar shear properties were also sensitive to the impact of curing pressure.

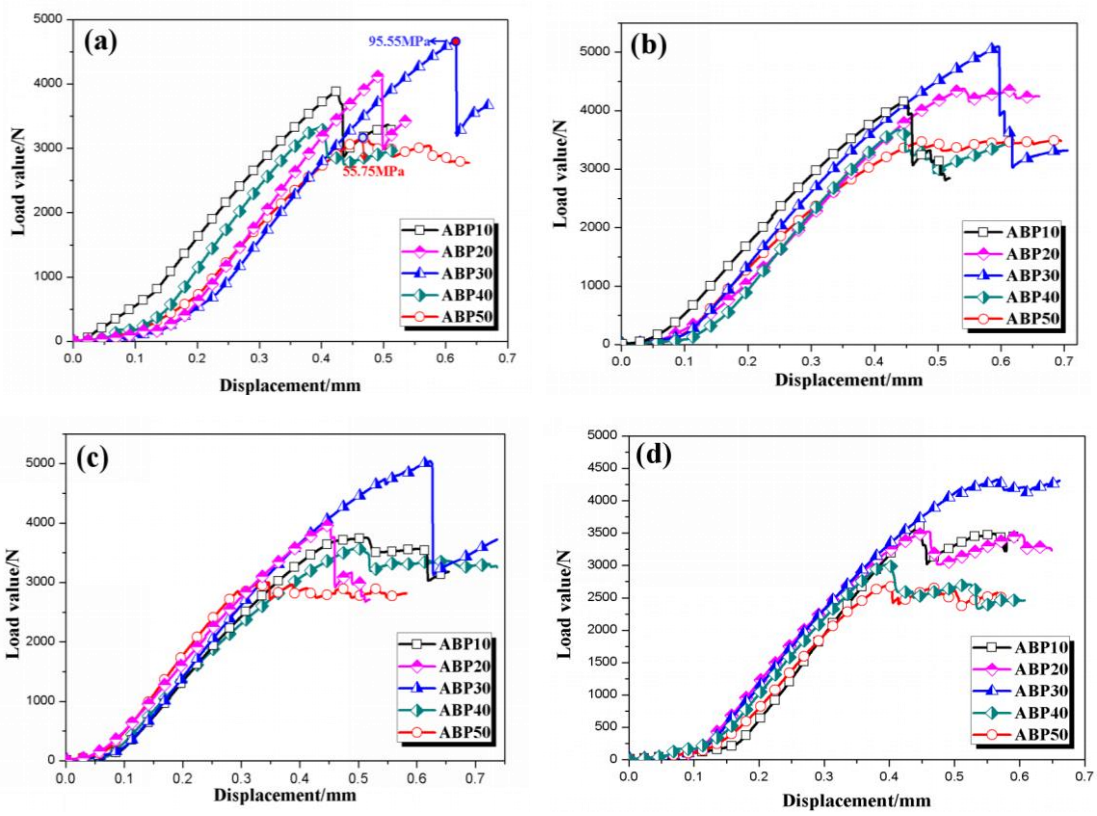

Fig. 14 Load-displacement curves of the NSFMLs under different experimental temperature: (a) room temperature; (b) 100 ℃; (c) 200 ℃ and (d) 300 ℃

Fig.15 exhibits the cross-sectional images of testing specimens with various fractions of B_4C particles under different experimental conditions. The testing specimens after DBS testing is shown in Fig.15(a), and the traces of loading location can be obviously observed on the surface of the specimens. The crack position occurred at the interface between the upper and central lower point as shown in Fig.15(b)-(f), which is coincident with the theoretical analysis of mechanics of the specimens under five-point supporting bending. It provides the advantage of the specimen having both high shear stresses and almost zero bending stresses over a substantial region of the specimen. In other words, the delamination location is the occurrence of interlaminar shear. The composite laminate contained with 30wt% of B_4C particles has the highest interlaminar shear value, and the main failure mainly occurred at the position between two unidirectional CFRP layers. But for the NSFMLs with 50wt% of B_4C particles, the destruction region mainly

concentrated on the interface between neutron shielding composite layer and AA6061 alloy plate. It is illustrated that for the NSFMLs with 30wt% of B_4C powder, the interlaminar shear strength between neutron shielding layer and AA6061 plate is higher than that between two unidirectional CFRP layer, while for the laminated composite with 50wt% of B_4C, the neutron shielding composite layer is inclined to be damaged. All specimens can satisfies the requirements of neutron shielding materials under thermal condition. The testing of ILS strength is to acquire the usage range of composite laminates at elevated temperature.

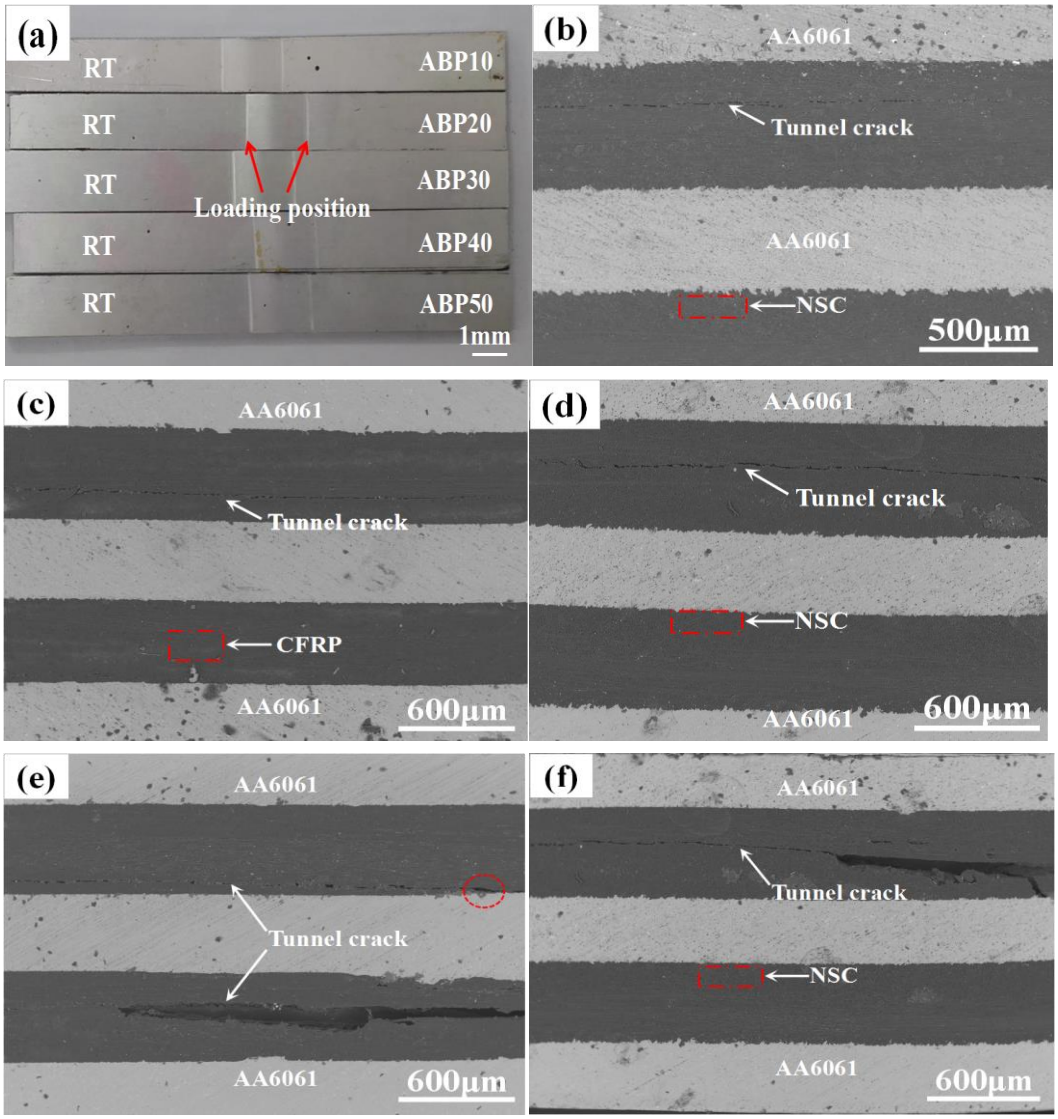

Fig.15 Images of (a) testing specimens with various contents of B_4C powder at room temperature and Cross-sectional graphs of the specimens containing (b) 10wt%, (c) 20wt%, (d) 30wt%, (e) 40wt% and (f) 50wt% of B_4C particles

4. Conclusions

This study investigated the thermal and mechanical properties of novel neutron shielding fibre metal laminates with 10wt%-50wt% of B_4C particles using hot molding process.

(1) Alkoxysilane coupling agent, uniform distribution of B_4C particles and interfacial bonding between particles and polyimide resin were crucial for the comprehensive properties

of NSFMLs.

(2) Composite laminates exhibited good thermal stability even when the experimental temperature approached to 300 ℃. It emerged obvious weight loss when the temperature exceeded over 400 ℃, owing to the pyrolysis of polyimide resin.

(3) Tensile strength of the NSFMLs decreased with the increasing of B_4C fraction and experimental temperature. The delamination between NSC layer and AA6061 plate happened in the process of tensile testing as a result of the discrepancy in the elongation of different materials.

(4) It was revealed that the addition of B_4C particles acting as a pinning effect can improve the resistance of relative movement between AA6061 plate and NSC layer, and the supporting and pinning synergistic effect hits a high point for composite laminates with 30wt% of B_4C particles. The specimens still kept good interlaminar shear strength even at 300 ℃.

Acknowledges

The authors gratefully acknowledge the financial support from the Fund of Jiangsu Innovation Program for Graduate Education, the Fundamental Research Funds for the Central Universities (No.KYLX_0258), Opening Project of Jiangsu Key Laboratory of Advanced Structural Materials and Application Technology (ASMA201401), and a Project Funded by the Priority Academic Program Development of Jiangsu Higher Education Institutions.

References

[1] R.J. Budnitz, Energ. Policy. 96 (2016) 735-739.

[2] Z. Csereklyeia, P.W. Thurnera, A. Bauerb, H. Küchenhoffb, Energ. Policy. 91 (2016) 49-59.

[3] X.P. Guo, X.D. Guo, Renew. Sust. Energ. Rev. 57 (2016) 999-1007.

[4] R. C. Ewing, Nat. Mater. 14 (2015) 252-257.

[5] J.L. Wang , Z. Wan, Prog. Nucl. Energ. 78 (2015) 47-55.

[6] S Tachimori, S Suzuki, Y Sasaki, Nippon Genshiryoku Gakkai-Shi. 43(2001) 1235-1241.

[7] K.L. Nash, G.J. Lumetta, Advanced separation techniques for nuclear fuel reprocessing and radioactive waste treatment, Elsevier, 2011.

[8] M.G. Bunn, J. Weeks, J.P. Horden, A.M. Macfarlane, S.E. Pickett, Harvard University, John F. Kennedy School of government and University of Tokyo, 2001.

[9] B. Bonin, The scientific basis of nuclear waste management, Handbook of Nuclear Engineering, Springer US, 2010: 3253-3419.

[10] A. Morioka, S. Sato, K. Ochiai, A. Sakasai, J. Hori, M. Yamauchi, T. Nishitani, A. Kaminaga, K. Masaki, S. Sakurai, T. Hayashi, M. Matsukawa, H. Tamai, S. Ishida, J. Nucl. Sci. Technol. 41 (2004) 109-112.

[11] A. Morioka, S. Sakurai, K. Okuno, S. Sato, Y. Verzirov, A. Kaminaga, T. Nishitani, H. Tamai, Y. Kudo, S. Yoshida, J. Nucl. Mater. 367 (2007) 1085-1089.

[12] J.W. Shin, J.W. Lee, S.G. Yu, B.K. Baek, J.P. Hong, Y.S. Seo, W.N. Kim, S.M. Hong, C.M. Koo, Thermochim. Acta. 585 (2014) 5-9.

[13] M. Saiyad, N.M. Devashrayee, R.K. Mevada, Polym. Composite. 35 (2014) 1263-1266.

[14] G. Odegard, M. Kumosa. Compos. Sci. Technol. 60 (2000): 2979-2988.

[15] Y.B. Hu, H.G. Li, L. Cai, J.P. Zhu, L. Pan, J. Xu, J. Tao, Compos. Part B-Eng. 69 (2015) 587-591.
[16] ASTM D3933-98, ASTM International, 2010.
[17] X.L. Fu, Y.B. Hu, H.G. Li, J. Tao, J. Nucl. Mater. 475 (2016) 227-236.
[18] ASTM D5470-12, ASTM International, 2006.
[19] G. Zhou, P.H. Nash, J. Whitaker, N. Jones, ECCM16-16TH European Conference on composite materials, 6 (2014) 22-26.
[20] Y.Q. Li, T. Qiu, Mat. Sci. Eng. A-Struct. 444 (2007) 184-191.
[21] H. Ji, D.P. Sellan, M.T. Pettes, X.H. Kong, J. Ji, L. Shi, R.S. Ruoff, Energ. Environ. Sci. 7 (2014) 1185-1192.
[22] G.L. Zhu, Y.P. Xiao, Y.X. Yang, J. Wang, B.D. Sun, R. BOOM, J. Shanghai Jiaotong Univ. (Sci.). 17 (2012) 257-262.
[23] X. Chen, J. Ren, N.W. Zhang, S.Y. Gu, J.B. Li, J. Reinf. Plast. Comp. 34 (2015) 28-36.
[24] J. Maljaars, F. Soetens, L. Katgerman, Metall. Mater. Trans. A. 39 (2008) 778-789.
[25] A.S. Yaghoubi, B. Liaw, Compos. Struct. 94 (2012) 2585-2598.